

CaMn_{0.9}Mg_{0.1}O_{3-δ} as Oxygen Carrier in a Gas-Fired 10 kW_{th} Chemical-Looping Combustion Unit

Malin Källén*, Magnus Rydén, Cristina Dueso, Tobias Mattisson, Anders Lyngfelt

Department of Energy and Environment

Chalmers University of Technology

SE-412 96, Gothenburg, Sweden

Abstract

Spray dried particles of the perovskite material CaMn_{0.9}Mg_{0.1}O_{3-δ} have been examined as oxygen carrier for chemical-looping combustion of natural gas. The experiments have been conducted in a continuously operating reactor with the nominal size 10 kW_{th}. The oxygen carrier particles showed excellent ability to convert fuel and complete combustion was reached at certain conditions. In general, the CO₂ yield increased with increased fuel reactor temperature and with increased circulation rate. The oxygen carrier was able to release gaseous oxygen through the so called CLOU-mechanism (Chemical-Looping with Oxygen Uncoupling). When the fuel reactor was fluidized by inert gas, there was oxygen release at temperatures above 700°C, reaching a maximum of more than 3% for temperatures above 850°C. Gas phase oxygen was also measured during operation with fuel, as long as the fuel conversion was complete. When the fuel reactor temperature was above 900°C and a high enough circulation rate was maintained, complete combustion of the fuel was achieved with an oxygen concentration in the outlet stream from the fuel reactor of more than 1%. This suggests that a substantial part of the fuel is converted by gaseous oxygen released from the particles. The oxygen carrier particles were subject to more than 350 h of fluidization, of which more than 175 h was at high temperature and more than 55 h with addition of fuel. The particles did not show any tendencies to form hard agglomerations or break down to fines due to attrition during the experiments. Operational problems included high rate of particle elutriation, which was likely an effect of a mismatch between the size and density of the particles, the air flow and the cyclone.

Keywords: chemical-looping combustion, chemical-looping with oxygen uncoupling, carbon capture and storage, fluidized bed combustion, perovskites

Nomenclature

AR	air reactor
CCS	carbon capture and storage
CI	circulation index (kg/min)
CLC	chemical-looping combustion
$CLOU$	chemical-looping with oxygen uncoupling
F_{ar}	inlet flow to air reactor (L_N/min)
F_{fr}	inlet flow to fuel reactor (L_N/min)
$(F_C)_{fuel}$	flow of carbon in fuel (L_N/min)
$(F_H)_{fuel}$	flow of hydrogen in fuel (L_N/min)
$(F_{O_2})_{air}$	flow of oxygen in air (L_N/min)
$(F_{O_2})_{fuel}$	flow of oxygen in fuel (L_N/min)
FR	fuel reactor
G_s	net solid flux ($\text{kg}/\text{m}^2\text{min}$)
Me	reduced oxygen carrier
MeO	oxidized oxygen carrier
u	superficial velocity (m/s)
u_t	terminal velocity of an average sized particle (m/s)
x_i	gas concentration, $i = \text{CO}, \text{CO}_2, \text{CH}_4$ (%)
γ_{CO_2}	CO_2 yield (-)
δ	degree of oxygen deficiency in a perovskite structure (-)
λ_{air}	air ratio (-)
ρ_{exit}	solids concentration at the riser exit (kg/m^3)

Introduction

Carbon dioxide capture and storage (CCS) is often mentioned as an important strategy to mitigate climate change. CCS is a method to reduce emissions of CO_2 to the atmosphere which consists of the separation of CO_2 from point-sources such as industries and power plants, i.e. the capture, transport to a storage location and long-term storage, for example in depleted gas fields or deep saline aquifers.

The most commonly proposed carbon dioxide capture technologies are pre-combustion capture, post-combustion capture and oxy-fuel combustion. In pre-combustion capture the fuel is reformed to carbon monoxide and hydrogen prior to combustion. The carbon monoxide is then reacted with steam to form carbon dioxide and more hydrogen. A gas separation unit is then necessary to separate the carbon dioxide and the hydrogen. In post-combustion capture the carbon dioxide is separated from the flue gases after combustion in a gas separation unit. In oxy-fuel combustion the fuel is burned in oxygen and recycled flue gases. An air separation unit is needed to produce pure oxygen from air.¹

Chemical-looping combustion (CLC) is a carbon dioxide capture technology that has developed very fast during the last ten years, see recent review articles by Lyngfelt et.al. and Adanez et.al.²³ It is often categorized as an oxy-fuel combustion technology, but it should rather be in a category of its own.

Background

In chemical-looping combustion, the oxygen needed for combustion of the fuel is supplied by a solid oxygen carrier. The oxygen carrier is oxidized by air in one reactor and reduced by the fuel in another reactor. The oxygen carrier particles are continuously circulated between the two reactors. In this way the carbon dioxide is inherently captured since the exhaust gas from the air reactor (AR) consists of oxygen depleted air and the exhaust gas from the fuel reactor (FR) ideally only consists of carbon dioxide and steam, of which the latter can easily be condensed to obtain an almost pure stream of carbon dioxide, see Figure 1.

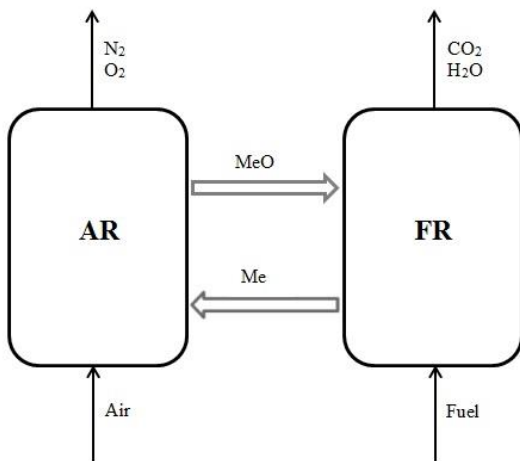


Figure 1. A schematic overview of the CLC process.

The fuel will react with the oxygen carrier according to:



The oxygen carrier will then be reoxidized in the air reactor according to:



The amount of energy released in the two reactions is equal to that for normal combustion of the same fuel. This is evident since the sum of reaction (1) and reaction (2) is normal combustion of the fuel with oxygen.

The most common approach to chemical-looping combustion is to use two interconnected fluidized beds. The oxygen carrier has the form of small particles and is circulated between the two beds. By using this method the gathered knowledge and experience from fluidized bed boilers (CFB) can be utilized.

Chemical-looping combustion was first thought of as a technology to produce carbon dioxide in a patent application in 1954.⁴ Later, the idea of using the process to capture carbon dioxide from combustion of fossil fuels was formed.⁵ The concept was proven feasible in 2004, when Lyngfelt and Thunman⁶ constructed and operated a 10 kW chemical-looping combustor for more than 100 h.

The development of oxygen carrier material is crucial to the progress of chemical-looping combustion. Some important criteria for oxygen carriers are:⁷

- High rates of oxidation and reduction.
- High oxygen transfer capacity.
- High mechanical integrity (low tendency for fragmentation and attrition).
- No tendency for agglomeration.
- Low cost.
- No harmful environmental or health effects.

Materials used as oxygen carriers are typically oxides based on nickel, copper, iron, manganese and cobalt. Suitable oxygen carriers were identified in a thermodynamic analysis.⁸ A comprehensive overview of investigated oxygen carrier materials can be found in the review articles by Lyngfelt and Mattisson⁹ and Adanez, Abad, Garcia-Labiano, Gayan and de Diego³.

Chemical-looping with oxygen uncoupling (CLOU) is a process closely related to chemical-looping combustion, which has been investigated by Mattisson, Lyngfelt and Leion¹⁰. The combustion of the fuel takes place in two steps. First the oxygen carrier releases gas phase oxygen according to:



The fuel can then be oxidized by gaseous oxygen instead of directly by the oxygen carrier. This is especially beneficial for solid fuels where char otherwise needs to be gasified to be able to react with the oxygen carrier. This is because char gasification is usually much slower compared to direct reaction between char and oxygen. CLOU could also prove to be favourable for gaseous

fuels, since the presence of gas phase O_2 could be expected to facilitate full combustion also without perfect mixing of gases and solids. In chemical-looping with oxygen uncoupling the char can instead react directly with gaseous oxygen released by the oxygen carrier. This process imposes some additional criteria for the oxygen carrier: ¹¹

- Be capable to take up and release oxygen under relevant conditions.
- Have sufficiently high rate of oxygen release.
- Have sufficiently high oxygen ratio.

Oxygen carrier materials based on copper oxide ^{12,13} manganese oxides ^{14,15} and combined materials such as $CaMnO_3$ ^{11,16} and $(Mn_yFe_{1-y})O$ ^{17,18} have been investigated for chemical-looping with oxygen uncoupling.

$CaMnO_{3-\delta}$ has a perovskite structure, i.e. it has a unit cell which can be written $ABO_{3-\delta}$ in which A represents the large cations and B the smaller cations. The δ -factor expresses the degree of oxygen deficiency in the structure and is zero for an ideal perovskite. This family of materials is interesting for chemical-looping applications because δ can be increased or reduced by altering factors in the surroundings such as temperature, pressure or O_2 partial pressure. ¹⁹ The surroundings in a chemical-looping air reactor are oxidizing, while they are reducing in the fuel reactor. Therefore δ_{ar} will be smaller and δ_{fr} will be larger. The amount of O_2 available for oxidation of fuel can be written as $(\delta_{fr} - \delta_{ar})$:



With respect to direct release of gas phase O_2 in inert atmosphere, different dynamics could be expected compared to materials which undergo distinct phase changes such as CuO . The latter is capable of providing constant O_2 concentration during reduction in inert gas, corresponding to equilibrium partial pressure of O_2 over $CuO-Cu_2O$ which is a function of temperature. In the case of $CaMnO_{3-\delta}$, the O_2 is released without distinct phase change according to reaction 4. Equilibrium O_2 partial pressure over $CaMnO_{3-\delta}$ is a function of the non-stoichiometry factor δ . With fully oxidized particles ($\delta=0$), O_2 can be released at comparably high concentrations. But as O_2 is removed from the perovskite structure and δ increases, the equilibrium O_2 partial pressure is continuously reduced in a logarithmic fashion. While it is possible to determine equilibrium curves for this kind of materials as function of temperature and δ -factor, this is complicated and outside the scope of this article. See the article by Leonidova et al. ²⁰ for a general discussion about this topic, and the paper by Rydén et al. ¹⁹ for a discussion about the implications for chemical-looping combustion.

It has previously been shown that materials based on $CaMnO_{3-\delta}$ are capable of releasing gas phase oxygen at temperatures and oxygen partial pressures relevant for chemical-looping with oxygen uncoupling. ²¹ A similar material, $CaMn_{0.875}Ti_{0.125}O_{3-\delta}$, has successfully been used as oxygen carrier for chemical-looping combustion experiments. ^{11,16}

The aim of this study was to improve and develop the CLOU process by examining an oxygen carrier with low cost and no harmful environmental effects.

Experimental

Oxygen Carrier

The oxygen carrier material used in this work was a perovskite structured material with the chemical formula $\text{CaMn}_{0.9}\text{Mg}_{0.1}\text{O}_{3-\delta}$ and was manufactured by VITO in Belgium. The raw materials were 46.8% manganese oxide, 50.5% calcium hydroxide and 2.7% magnesium oxide of commercial grades. Particles were produced by spray drying, followed by calcination at 1300°C for 4 h.

The crushing strength of the fresh particles was 1.38 N, which is the average force needed to crush a particle in the size span 180-250 μm . An XRD scan identified CaMnO_3 and MgO as the present phases in the fresh particles and the bulk density was measured to 1932 kg/m^3 . The size distribution of the fresh particles can be seen in Figure 2.

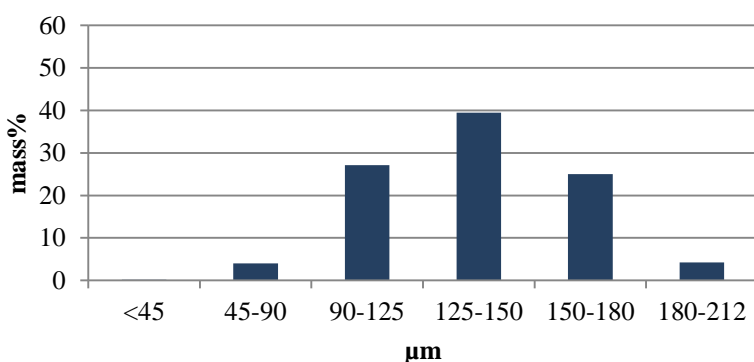


Figure 2. The size distribution of the fresh oxygen carrier particles.

Experimental Setup

The experiments were carried out in a $10 \text{ kW}_{\text{th}}$ CLC pilot plant for gaseous fuels. It was designed and built in the EU-project GRACE in 2002-2003.²² Natural gas with a composition equivalent of $\text{C}_{1.14}\text{H}_{4.25}\text{O}_{0.01}\text{N}_{0.005}$ was used as fuel, see Table 1 for the species composition.

Table 1. The annual average composition for 2012 of the natural gas as reported by the gas supplier.

Species	Mole%
Methane	88.84
Ethane	6.11
Propane	2.44
Isobutane	0.37
n-Butane	0.54
Isopentane	0.13
n-Pentane	0.08
Hexane+	0.06
Nitrogen	0.36
Carbon Dioxide	1.06

The reactor system consists of two interconnected fluidized beds, one of which constitutes the air reactor and the other one the fuel reactor. A schematic picture of the experimental setup can be seen in Figure 3. This experimental setup has previously been used by Lyngfelt, Kronberger, Adanez, Morin and Hurst ²², Lyngfelt and Thunman ⁶, Linderholm, Abad, Mattisson and Lyngfelt ²³ and Linderholm, Mattisson and Lyngfelt ²⁴ using nickel-based oxygen carrier materials.

The air reactor has an inner diameter of 150 mm. A riser is connected to the air reactor and it is the gas velocity in the air reactor and the riser which creates the driving force for the circulation. The separation of gas and particles is managed by a cyclone after the riser. The particles are brought from the cyclone to the fuel reactor through a downcomer and a loop seal. This assures that no gas will leak into the fuel reactor. The fuel reactor consists of a bubbling fluidized bed which is fluidized by the gaseous fuel. The lower part of the fuel reactor has an inner diameter of 150 mm and the higher part has an inner diameter of 260 mm. Particles leave the fuel reactor via an overflow exit, and fall down into a second particle seal leading back in to the air reactor. There is a vertical plate attached inside the fuel reactor which prevents particles entering the bed to by-pass the bed to the overflow exit. Thus, the solids flow will first go downwards on one side of this plate, turn and go upwards on the other side. This plate was not present in previous experimental campaigns with this unit. The height from the bottom of the air reactor to the top of the riser is 2230 mm.

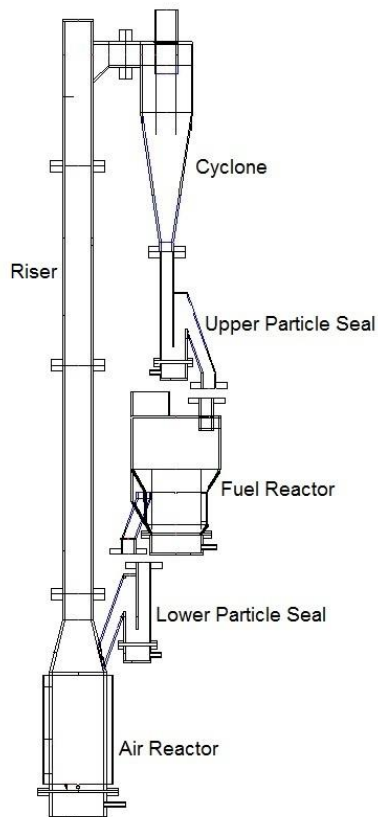


Figure 3. A schematic picture of the experimental setup.

The air reactor is fluidized by air preheated to 1000°C and both particle seals are fluidized by nitrogen. The nitrogen used to fluidize the particle seals will escape through both the air reactor and the fuel reactor and thus dilute both exhaust gas streams. To avoid the nitrogen dilution, the particle seals can be fluidized by steam instead. This option was not utilized during these experiments though.

The exhaust gas stream leaving the cyclone is first led through finned pipes for passive cooling, then a part of the stream is led on to the gas conditioning system and the gas analysers, and the remaining gas is led through a bag filter. The exhaust gas stream from the fuel reactor is also led through finned pipes before a part of the stream is led to the gas conditioning system and the gas analysers, and the remaining gas passes a water seal, where the steam condensate is collected and elutriated particles are captured.

The gas analysers measure the concentration of CO₂, CO, CH₄ and O₂ from the fuel reactor and the concentrations of O₂ and CO₂ from the air reactor. The carbon containing species are measured with IR instruments and the oxygen is measured with paramagnetic technique. The temperature is measured with thermocouples at eight points in the reactor system, three in the air reactor, one in the riser, one in the cyclone, one in the higher particle seal and two in the fuel reactor. Pressure drops in the reactor systems are measured by 20 pressure transducers. The

pressure drops are measured in order to be able to assess the fluidization behaviour and the particle inventory in different parts of the reactor system. Gas concentrations, temperatures and pressure drops are logged every ten seconds.

A supervision system is used to be able to operate the system during nights. If temperature or gas concentrations are not kept within certain accepted intervals, the supervision system will shut off the fuel flow to the fuel reactor and replace it with nitrogen.

Data Evaluation

The exhaust gas concentrations were measured on dry basis since steam is condensed prior to measurement. In order to facilitate the analysis, an estimated value of the concentration of H₂ in dry gas, $x_{H_2,fr}$, was calculated. This was done by solving the species balance over the reactor, assuming that there was no formation of solid carbon and that the gas composition from the fuel reactor corresponded to thermodynamic equilibrium for the water-gas shift reaction. A detailed description of the methodology for these calculations can be found elsewhere.²⁵ The cited study involved highly catalytically active NiO-based oxygen carrier particles. It shall be acknowledged that it is not obvious that the gas concentrations will be at perfect equilibrium in the current study. The examined oxygen carrier could be expected to be slightly more reactive with H₂ compared to CO. However, previous experiments with similar materials in a high-temperature steel reactor, in which gas composition was double checked with a gas chromatograph, indicated that results close to equilibrium was reached anyway.¹¹

The circulation rate has been calculated to evaluate the operating conditions in the system. The following expression, previously used by Linderholm, Abad, Mattisson and Lyngfelt²³ for this unit, has been used to calculate the net solid flux:

$$G_s = \rho_{exit}(u - u_t) = -\frac{1}{g} \frac{dp}{dh}(u - u_t) \quad (5)$$

The net solids flux calculated by this expression is believed to be a slight overestimation, but it is still a useful measure for comparing particle circulations. The net solid flux multiplied with the cross sectional area of the riser is referred to as circulation index (CI) expressed in kg/min.

To evaluate the experiments the CO₂ yield was calculated. The CO₂ yield is defined as the amount of carbon dioxide formed divided by the total amount of carbon species in the outlet flow according to:

$$Y_{CO_2} = \frac{x_{CO_2}}{x_{CO_2} + x_{CO} + x_{CH_4}} \quad (6)$$

The CO₂ yield is very close to the combustion efficiency when using natural gas as fuel. This is because the heating value of natural gas is almost equal to that for carbon monoxide and the corresponding amount of hydrogen.

Results and Discussion

The CaMn_{0.9}Mg_{0.1}O_{3-δ} particles have been fluidized for more than 350 h in the reactor system. 120 h of these were under hot conditions, i.e. the temperature in the fuel reactor was over 600°C. The experiments with fuel were conducted during 55 h of the 120h in hot conditions. An overview of the experiments can be seen in Table 2.

Table 2. An overview of the performed experiments.

Day	Time fluidized [h]	Time under hot conditions [h]	Time with fuel [h]	Particle inventory [kg]	Air flow [L _N /min]	Fuel flow [L _N /min]
1	1.0	0.0	0.0	13	600	0
2	6.2	0.0	0.0	15	200	0
3	29.5	0.0	0.0	15	200	0
4	8.5	6.5	0.0	15	100-260	0
5	27.6	7.1	3.2	15	180-200	7.5–12
6	41.7	8.5	4.1	15	200	9-12
7	32.2	2.3	0.0	15	200	0
8	31.3	19.5	8.0	15	200	12
9	40.2	20.0	16.8	17	150-200	9-12
10	42.4	24.0	13.7	17	160	7.5–12
11	30.7	5.2	0.9	17	200	12
12	11.7	6.1	2.8	17	120-200	6-9
13	47.4	20.3	6.4	17	200	15
Sum:	350.2	119.5	55.8			

The particle inventory has been varied between 13 and 17 kg. At the time the system was opened, 5 kg of particles were found in the fuel reactor. As the fuel reactor has an overflow exit, the fuel reactor inventory is believed to have been fairly constant during the experiments.

Oxygen Release

The oxygen carrier particles were capable of releasing gas phase oxygen above certain temperatures when the fuel reactor was fluidized with nitrogen gas. This is demonstrated in Figure 4, where the oxygen concentration in the fuel reactor is shown as a function of the temperature in the fuel reactor. In Figure 4 it can be seen that the O₂ uncoupling is increased at higher temperature. This is believed to be the effect of two mechanisms. Firstly, the thermodynamic equilibrium moves towards higher oxygen partial pressure at higher temperatures and secondly, the kinetics for chemical reactions will generally be faster at higher temperatures.

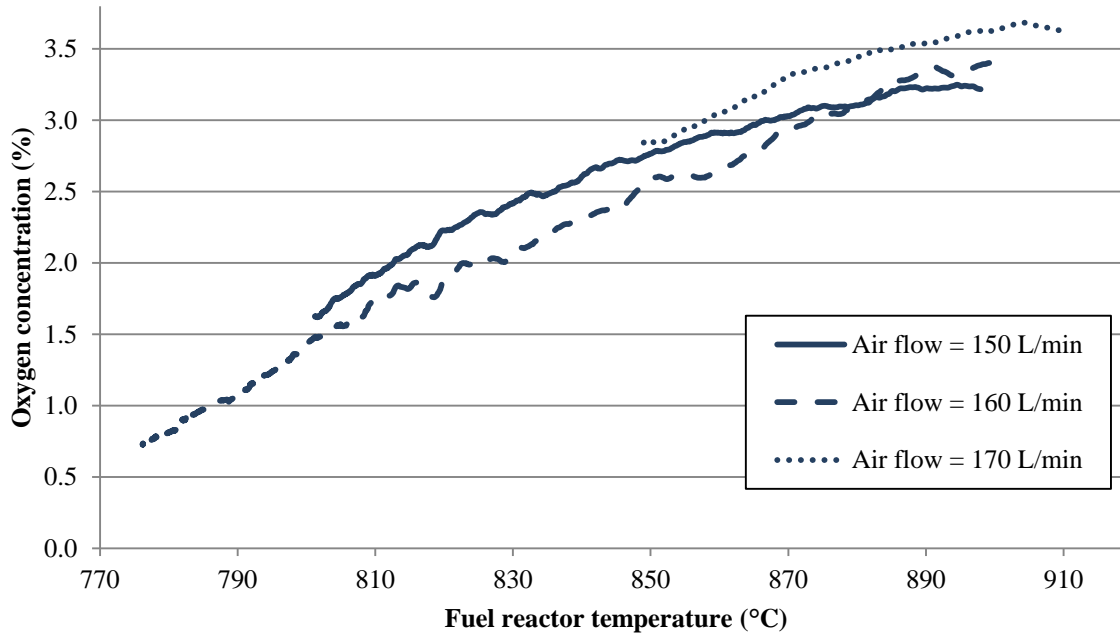


Figure 4. O₂ concentration in the fuel reactor as a function of the fuel reactor temperature with $F_{ar} = 150 \text{ L}_N/\text{min}$, $F_{ar} = 160 \text{ L}_N/\text{min}$ and $F_{ar} = 170 \text{ L}_N/\text{min}$ and $F_{fr} = 35 \text{ L}_N/\text{min N}_2$. These results were obtained during day 9, 10 and 12.

Combustion Experiments

The experimental campaign was performed under a number of continuous series summarized in Table 2. The longest continuous experiment with fuel lasted for more than 16 h. The gas concentrations at the outlet from the fuel reactor, fuel reactor temperature and CO₂ yield during this experiment can be seen in Figure 5. Fuel operation was started at time = 0 in the figure and the dashed, vertical line indicates a change of the fuel flow from 12 L_N/min to 9 L_N/min and a change of the air flow from 150 L_N/min to 200 L_N/min. Although stable operation is reached, the CO₂ yield and fuel reactor temperature are slowly decreasing. The reason is that the particle inventory is gradually decreasing because particles are elutriated to the filter. As can be seen in the figure, the decreased CO₂ yield involves increasing concentrations of CO, H₂ and CH₄. A magnification of the concentration profiles for CO, CH₄ and O₂ can be seen in Figure 6.

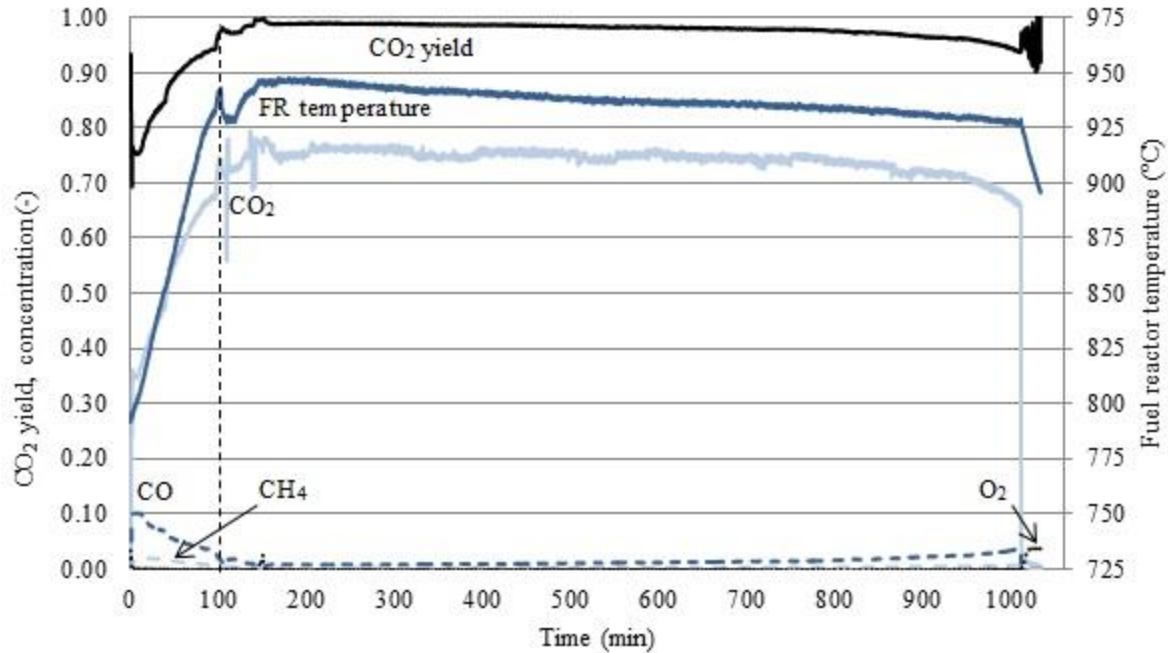


Figure 5. Gas concentrations at the outlet of the fuel reactor, fuel reactor temperature and CO₂ yield as a function of time with $F_{ar} = 150 \text{ L}_N/\text{min}$ and $F_{fr} = 12 \text{ L}_N/\text{min}$ (8.8 kW) before the dashed line and $F_{ar} = 200 \text{ L}_N/\text{min}$ and $F_{fr} = 9 \text{ L}_N/\text{min}$ (6.6 kW) after the dashed line. Note that the fuel reactor temperature has a separate y-axis. These results were obtained during day 9.

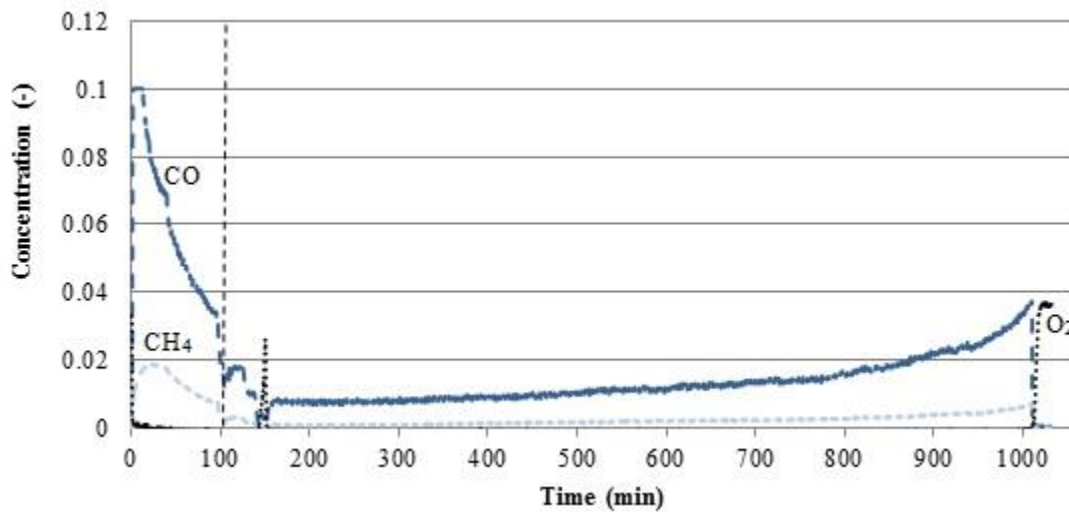


Figure 6. Gas concentrations at the outlet of the fuel reactor as a function of time with $F_{ar} = 150 \text{ L}_N/\text{min}$ and $F_{fr} = 12 \text{ L}_N/\text{min}$ (8.8 kW) before the dashed line and $F_{ar} = 200 \text{ L}_N/\text{min}$ and $F_{fr} = 9 \text{ L}_N/\text{min}$ (6.6 kW) after the dashed line. These results were obtained during day 9.

After approximately 16.7 h, the CO concentration was higher than the accepted interval and the supervision system shut the fuel flow and started fluidizing of the fuel reactor with nitrogen. This caused instantaneous drops in gas concentrations and fuel reactor temperature. As can be seen in the right corner of Figure 6, the oxygen concentration in the fuel reactor increased to almost 4%.

This is due to oxygen release from the oxygen carrier particles when oxygen was no longer consumed in the combustion reactions.

The decrease in CO_2 yield and thus the increase in hydrogen and carbon monoxide concentrations are caused by a steady decrease in particle inventory in the whole reactor system. The particles are elutriated to the filter after the cyclone which results in a lower solids circulation. The circulation rate is steadily decreasing during experiment, which can be seen in Figure 7.

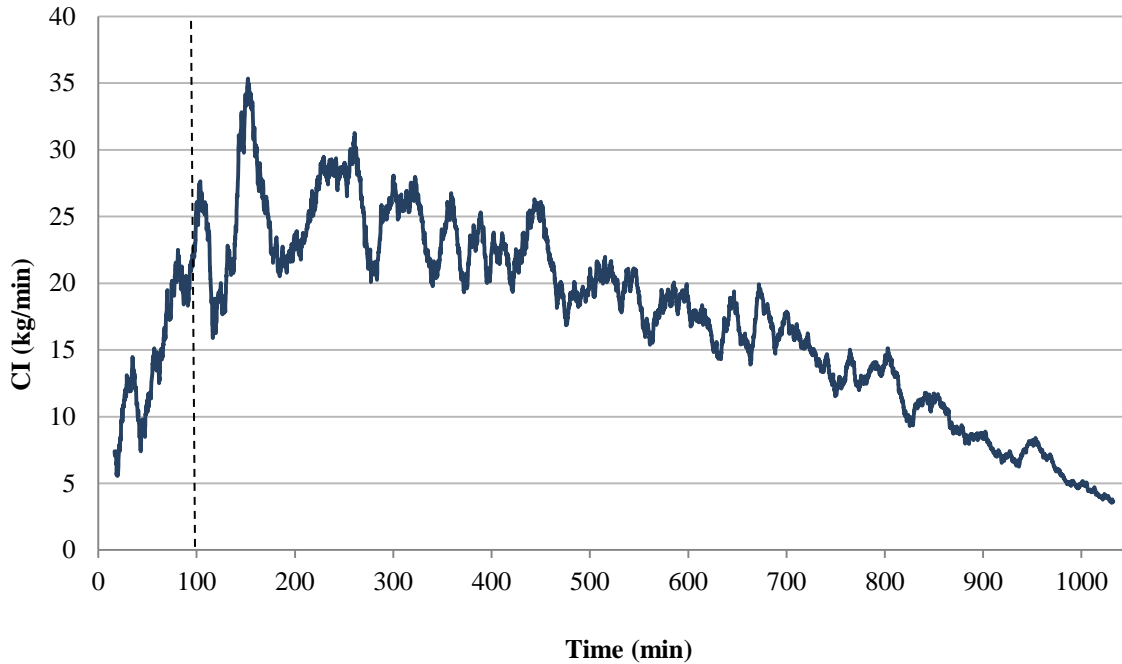


Figure 7. The circulation index as a function of time with $F_{\text{ar}} = 150 \text{ L}_\text{N}/\text{min}$ and $F_{\text{fr}} = 12 \text{ L}_\text{N}/\text{min}$ (8.8 kW) before the dashed line and $F_{\text{ar}} = 200 \text{ L}_\text{N}/\text{min}$ and $F_{\text{fr}} = 9 \text{ L}_\text{N}/\text{min}$ (6.6 kW) after the dashed line. The line represents the moving average for 100 points. These results were obtained during day 9.

Effect of Fuel Reactor Temperature

Experiments with fuel were performed with varying air and fuel flow as shown in Table 2. The CO_2 yield as a function of fuel reactor temperature for different air and fuel flows can be seen in Figure 8. All three experiments were performed during heat up with fuel. Note that the temperature level is lower for Figure 8a.

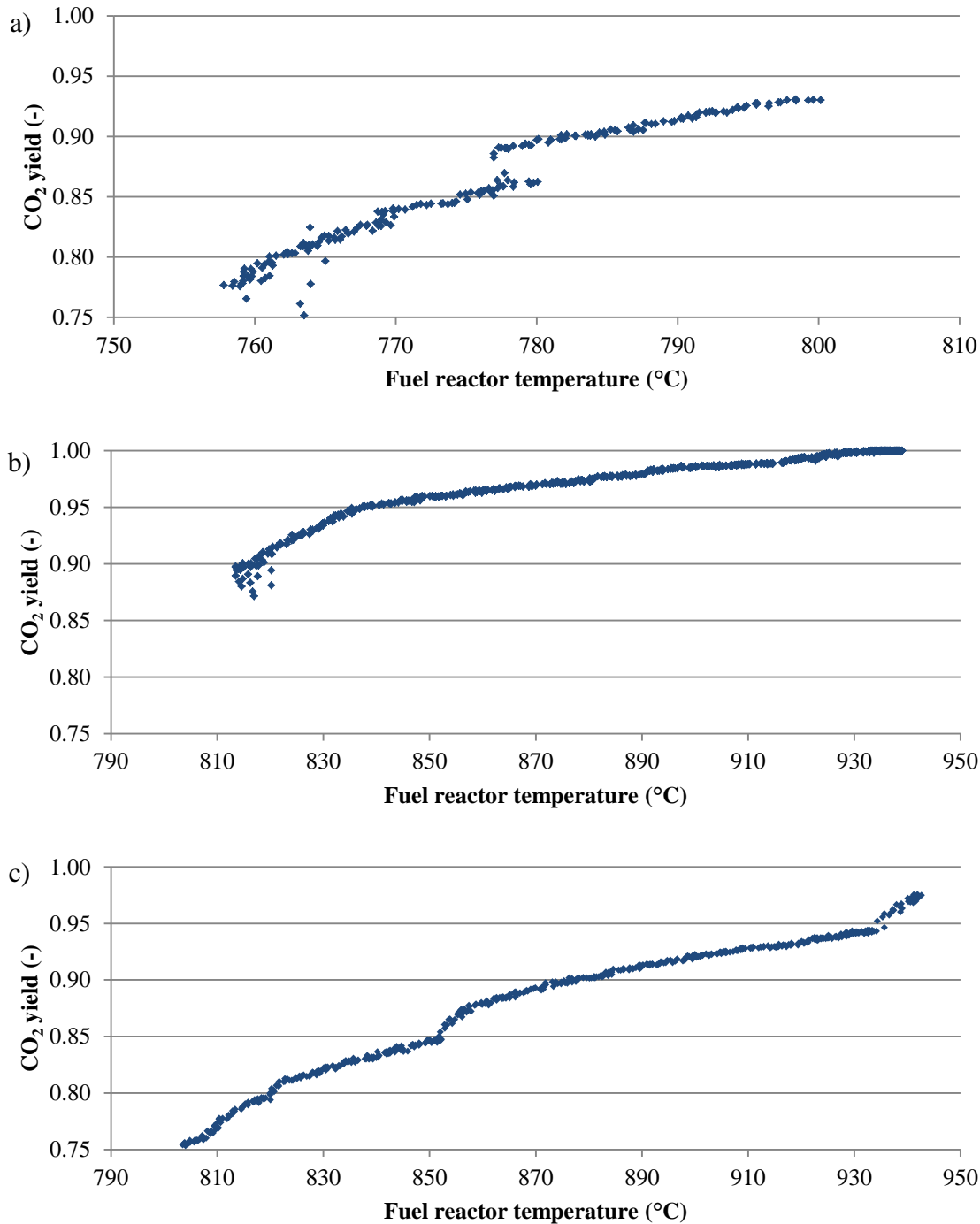


Figure 8. CO₂ yield as a function of fuel reactor temperature with a) $F_{ar} = 200 \text{ L}_N/\text{min}$ and $F_{fr} = 7.5 \text{ L}_N/\text{min}$ (5.5 kW) during day 5 b) $F_{ar} = 200 \text{ L}_N/\text{min}$ and $F_{fr} = 9 \text{ L}_N/\text{min}$ (6.6 kW) during day 6 c) $F_{ar} = 150 \text{ L}_N/\text{min}$ and $F_{fr} = 12 \text{ L}_N/\text{min}$ (8.8 kW) during day 9.

Figure 8 clearly shows the CO₂ yield dependence on fuel reactor temperature. When comparing Figure 8b) and Figure 8c) it can also be seen that the gas flows affect the CO₂ yield. Whereas the CO₂ yield reaches 1 at 930°C for an air flow of 200 L_N/min and a fuel flow of 9 L_N/min, the CO₂

yield is only 0.94 at the same temperature for an air flow of 149 L_N/min and a fuel flow of 12 L_N/min. A variation in air flow will give a variation in solids circulation and a variation in fuel flow will give a variation in solids inventory in the fuel reactor related to fuel power.

Effect of Fuel Flow and Circulation Rate

In Figure 9, the gas concentrations at the outlet from the fuel reactor are shown as a function of time. The experiment was conducted at stable operation and the changes in gas concentration are due to changes of the fuel flow only. The fuel flows for the respective periods are shown in the figure. It can be seen in the figure that a fuel flow of 9 L_N/min results in oxygen release in the fuel reactor and that higher fuel flows do not give a surplus of oxygen in the fuel reactor. When no gaseous oxygen is measured in the fuel reactor, the combustion is not complete. As can be seen in Figure 9, the concentrations of carbon monoxide and methane are above zero for higher fuel flows. The changes in fuel flow do also change the air ratio as the air flow is kept constant. In this experiment a fuel flow of 9 L_N/min correspond to an air ratio of 2.1, a fuel flow of 11 L_N/min to an air ratio of 1.8 and a fuel flow of 12 L_N/min to an air ratio of 1.6. In this case the air flow was kept constant in order to keep the circulation rate constant as well.

The relationship between CO₂ yield and fuel flow is investigated in Figure 10. The figure shows that an increased fuel flow will give lower CO₂ yield. By comparing Figure 9 and Figure 10, it can be seen that when the air flow is 200 L_N/min, the combustion is complete for a fuel flow of 9 L_N/min, whereas when the air flow is 160 L_N/min, the CO₂ yield reaches only 98% for the same fuel flow.

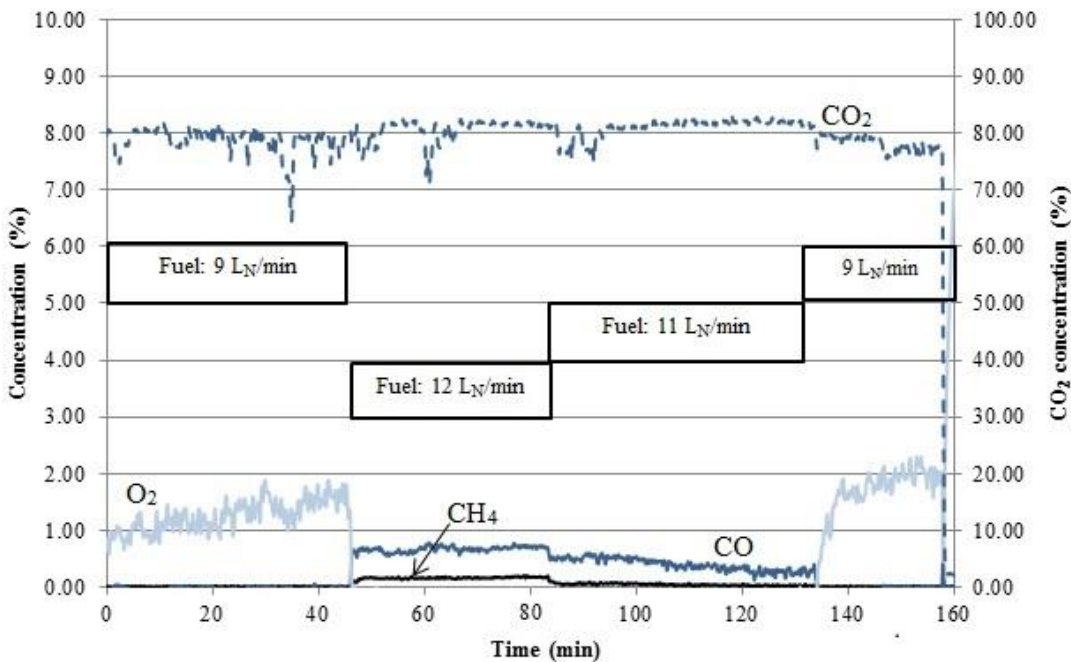


Figure 9. The gas concentrations at the outlet of the fuel reactor as a function of time with $F_{ar} = 200$ L_N/min, $F_{fr} = 9-12$ L_N/min (6.6-8.8 kW) and $T_{fr} = 935-955^{\circ}\text{C}$. Note that the concentrations of CO₂ have a separate y-axis. These results were obtained during day 6.

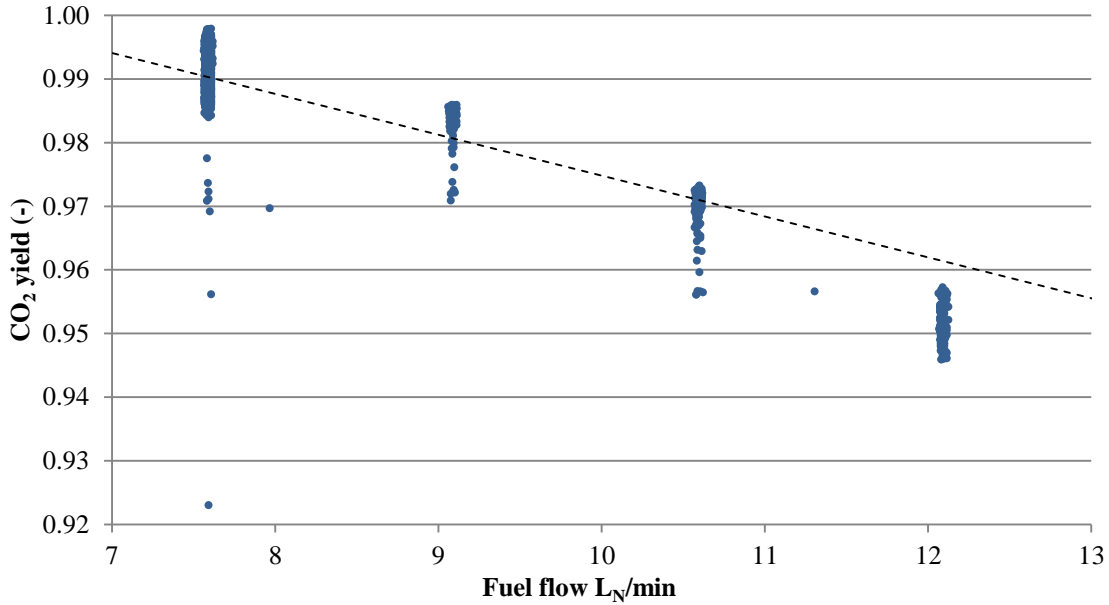


Figure 10. CO₂ yield as a function of fuel flow for a fuel reactor temperature of 930-950°C and $F_{ar} = 160 \text{ L}_N/\text{min}$. These results were obtained during day 10.

This effect of the air flow can be explained by that the circulation rate in the system is dependent on the air flow. In Figure 11 the CO₂ yield is expressed as a function of circulation index. As can be seen in the figure, a higher circulation index gives a higher CO₂ yield.

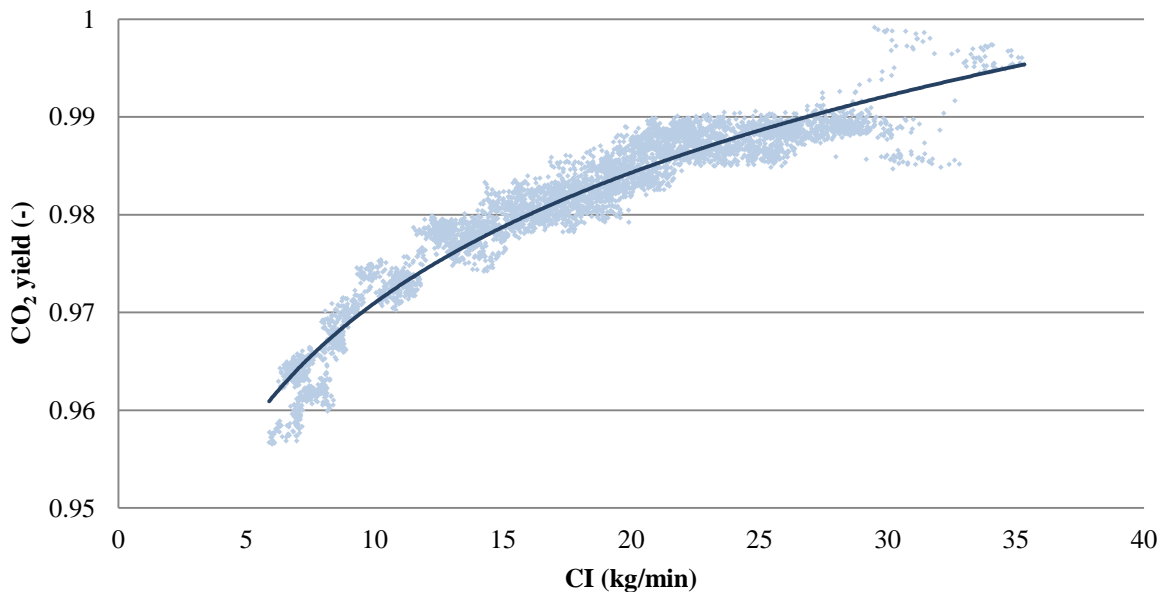


Figure 11. CO₂ yield as a function of circulation index with $F_{ar} = 170 \text{ L}_N/\text{min}$ and $F_{fr} = 9 \text{ L}_N/\text{min}$ at a fuel reactor temperature of 930-950°C. These results were obtained during day 9.

As can be seen in Figure 7, the circulation index reached a maximum at around 150 min during day 9. This peak coincides with full fuel conversion and release of oxygen, as can be seen in Figure 6. The gas concentration during the time period for this peak is shown in greater detail in Figure 12. As the moving average of the circulation index reached a maximum of 35 kg/min at around 150 min, the methane is fully converted and an excess oxygen gas concentration is measured in the fuel reactor. Worth noting is also that there is a short time period after 140 min where the concentrations of methane and oxygen are zero and the concentration of carbon monoxide is below 0.5%. This is desirable, since these conditions would give an exhaust stream of very pure carbon dioxide after steam condensation if all loop seals are fluidized with steam.

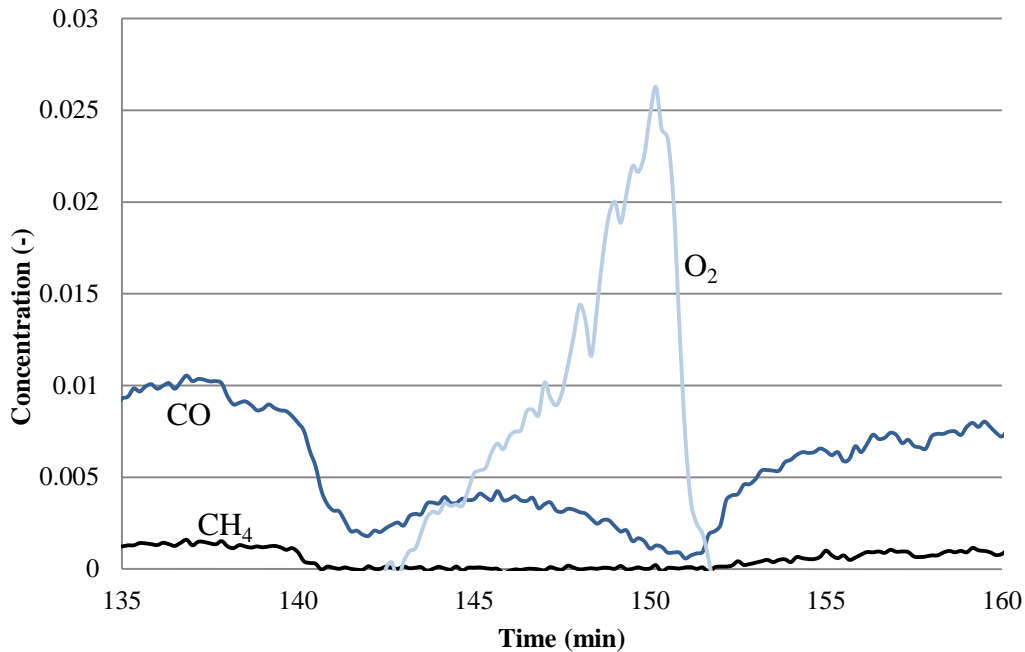


Figure 12. The gas concentrations at the outlet of the fuel reactor with $F_{ar} = 200 \text{ L}_N/\text{min}$ and $F_{fr} = 9 \text{ L}_N/\text{min}$ (6.6 kW) during a peak in circulation index. These results were obtained during day 9.

Finally, it shall be mentioned that this campaign of experiments has been affected by the fact that the oxygen particles used were of a smaller size distribution than this reactor unit was designed for. The mean particle size interval was 90-125 μm , whereas the mean particle size interval has been 125-180 μm in earlier studies done in this reactor unit. Furthermore, the bulk density for the particles used in this study is lower than that for previously used particles. The main problem occurred in the cyclone, which gave a poor performance for the too small and light particles. Several attempts were made to run fuel experiments overnight, which caused more than a third of the particle inventory to end up in the filter after the cyclone.

Particle Agglomeration and Attrition

The oxygen carrier particles showed good fluidization properties throughout the experiments. During one experiment, the supervision system was triggered to stop the fuel flow due to a stop in circulation. Analysis of pressure measurements clearly indicated that the operation problem was caused by a stop in the cyclone exit or cyclone leg. The circulation restarted by itself after

approximately 4 h and the particles fluidized properly again. To be noted is that the material worked well despite being stuck a long period at high temperature. It is believed that no lasting agglomerates were formed. However, at the time the fuel reactor was opened, a smaller amount of agglomerates were found, see Figure 13. Some of the agglomerates had a reddish colour and all of them had a diameter of 1-2 cm and were easily crushed between the fingertips.



Figure 13. Photo of some of the agglomerates found in the fuel reactor.

There has been little evidence of particle attrition during the experiments. As very large amounts of oxygen carrier particles were elutriated to the particle filters, it was not possible to sieve all of them before reintroducing them to the system. Instead two samples of 300 g were sieved after each filter emptying and the particle size distribution was noted. The mass fraction of fines, i.e. particles smaller than 45 μm , at each filter cleaning can be seen in Figure 14. As can be seen in the figure, the production of fines was very low and decreased during the experimental campaign.

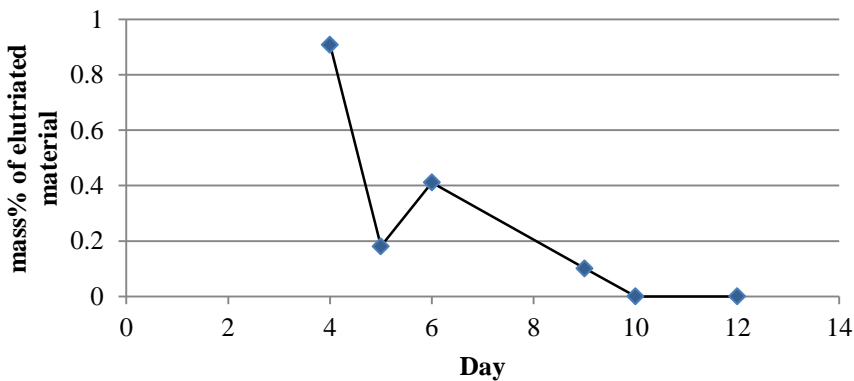


Figure 14. The mass fraction of fines, $<45\mu\text{m}$, for the sieved samples of elutriated material.

The material loss during operation with fuel was typically 0.32 kg/h and the mass fraction of fines was 0-0.4% from the first fuel addition on day 5. The highest mass fraction of fines obtained with fuel addition, i.e. 0.4%, would mean a loss of fines of 0.0085 mass%/h, which corresponds to a lifetime of 12 000 h. It should be noted that these numbers are indicative of a very low attrition, but that the exact numbers are uncertain due to the high elutriation combined with low fraction of fines.

Conclusions

$\text{CaMn}_{0.9}\text{Mg}_{0.1}\text{O}_{3-\delta}$ has been examined as oxygen carrier in chemical-looping combustion in a continuously operating test reactor with natural gas as fuel. The particles have been fluidized at hot conditions for 120 h and of which 55 h with fuel addition. The following conclusions can be drawn from the experiments:

- $\text{CaMn}_{0.9}\text{Mg}_{0.1}\text{O}_{3-\delta}$ shows great promise as an oxygen carrier for chemical-looping with oxygen uncoupling. The material did not show tendency for agglomeration or attrition and it releases oxygen (above 3% in oxygen concentration) at relevant conditions.
- The CO_2 yield is temperature dependent and increases with increased temperature.
- The CO_2 yield is also dependent on circulation rate and increases with increased circulation rate.
- At stable operation above 900°C the CO_2 yield is in the range of 0.98-1. Complete fuel conversion was only seen in presence of oxygen; the highest conversion without oxygen present was above 99.5%.
- The formation of fines was very small, estimated to be below 0.01%, indicating that the lifetime of the particles could be very long.

Compared to previous successful results in this unit with nickel-based materials, these results indicate higher conversion and similar low loss of fines. Moreover the material used in this study is based on less costly raw materials, and is also more benign with respect to health and environment.

Acknowledgements

The research leading to these results has received funding from the Seventh Framework Programme under grant agreement n° 241401. C. Dueso would also like to acknowledge the Spanish Ministry of Education.

References

- (1) IPCC "IPCC Special Report on Carbon Dioxide Capture and Storage," 2005.
- (2) Lyngfelt, A.: Oxygen Carriers for Chemical Looping Combustion - 4 000 h of Operational Experience. *Oil Gas Sci. and Technol.* **2011**, 66, 2.
- (3) Adanez, J.; Abad, A.; Garcia-Labiano, F.; Gayan, P.; de Diego, L. F.: Progress in Chemical-Looping Combustion and Reforming technologies. *Prog. Energy Combust. Science* **2012**, 38, 215-282.
- (4) Lewis, W. K.; Gilliland, E. R.: Production of pure carbon dioxide. patent, U., Ed.: USA, 1954.
- (5) Ishida, M.; Jin, H.: A novel combustor based on chemical-looping reactions and its reaction kinetics. *J. Chem. Eng. Jpn.* **1994**, 27, 296-301.
- (6) Lyngfelt, A.; Thunman, H.: Chapter 36 - Construction and 100 h of Operational Experience of A 10-kW Chemical-Looping Combustor. In *Carbon Dioxide Capture for Storage in Deep Geologic Formations*; Elsevier Science: Amsterdam, 2005; pp 625-645.
- (7) Johansson, E.; Mattisson, T.; Lyngfelt, A.; Thunman, H.: A 300 W laboratory reactor system for chemical-looping combustion with particle circulation. *Fuel* **2006**, 85, 1428-1438.
- (8) Jerndal, E.; Mattisson, T.; Lyngfelt, A.: Thermal Analysis of Chemical-Looping Combustion. *Chem. Eng. Res. Des.* **2006**, 84, 795-806.
- (9) Lyngfelt, A.; Mattisson, T.: Materials for chemical-looping combustion. In *Power Engineering for CCS Power Plants*; WILEY-VCH Verlag, 2011.
- (10) Mattisson, T.; Lyngfelt, A.; Leion, H.: Chemical-looping with oxygen uncoupling for combustion of solid fuels. *Int. J. Greenhouse Gas Control* **2009**, 3, 11-19.
- (11) Rydén, M.; Lyngfelt, A.; Mattisson, T.: $\text{CaMn}_{0.875}\text{Ti}_{0.125}\text{O}_3$ as oxygen carrier for chemical-looping combustion with oxygen uncoupling (CLOU)—Experiments in a continuously operating fluidized-bed reactor system. *Int. J. Greenhouse Gas Control* **2011**, 5, 356-366.
- (12) Mattisson, T.; Leion, H.; Lyngfelt, A.: Chemical-looping with oxygen uncoupling using CuO/ZrO_2 with petroleum coke. *Fuel* **2009**, 88, 683-690.
- (13) Gayán, P.; Adánez-Rubio, I.; Abad, A.; de Diego, L. F.; García-Labiano, F.; Adánez, J.: Development of Cu-based oxygen carriers for Chemical-Looping with Oxygen Uncoupling (CLOU) process. *Fuel* **2012**, 96, 226-238.
- (14) Shulman, A.; Cleverstam, E.; Mattisson, T.; Lyngfelt, A.: Manganese/Iron, Manganese/Nickel, and Manganese/Silicon Oxides Used in Chemical-Looping With Oxygen Uncoupling (CLOU) for Combustion of Methane. *Energy Fuels* **2009**, 23, 5269-5275.
- (15) Shulman, A.; Cleverstam, E.; Mattisson, T.; Lyngfelt, A.: Chemical – Looping with oxygen uncoupling using Mn/Mg-based oxygen carriers – Oxygen release and reactivity with methane. *Fuel* **2011**, 90, 941-950.

- (16) Leion, H.; Larring, Y.; Bakken, E.; Bredesen, R.; Mattisson, T.; Lyngfelt, A.: Use of $\text{CaMn}_{0.875}\text{Ti}_{0.125}\text{O}_3$ as oxygen carrier in chemical-looping with oxygen uncoupling. *Energy Fuels* **2009**, *23*, 5276-5283.
- (17) Azimi, G.; Rydén, M.; Leion, H.; Mattisson, T.; Lyngfelt, A.: $(\text{Mn}_z\text{Fe}_{1-z})_y\text{O}_x$ combined oxides as oxygen carrier for chemical-looping with oxygen uncoupling. *AIChE J.* **2012**.
- (18) Rydén, M.; Lyngfelt, A.; Mattisson, T.: Combined manganese/iron oxides as oxygen carrier for chemical looping combustion with oxygen uncoupling (CLOU) in a circulating fluidized bed reactor system. Amsterdam, 2011; Vol. 4; pp 341-348.
- (19) Rydén, M.; Leion, H.; Mattisson, T.; Lyngfelt, A.: Combined oxides as oxygen carrier for chemical-looping with oxygen uncoupling. In *2nd International Conference on Chemical Looping*; Darmstadt, 2012.
- (20) Leonidova, E. I.; Leonidov, I. A.; Patrakeev, M. V.; Kozhevnikov, V. L.: Oxygen non-stoichiometry, high-temperature properties, and phase diagram of $\text{CaMnO}_{3-\delta}$. *J. Solid State Electrochem.* **2011**, *15*, 1071-1075.
- (21) Bakken, E.; Norby, T.; Stølen, S.: Nonstoichiometry and reductive decomposition of $\text{CaMnO}_{3-\delta}$. *Solid State Ionics* **2005**, *176*, 217-223.
- (22) Lyngfelt, A.; Kronberger, B.; Adanez, J.; Morin, J. X.; Hurst, P.: - The grace project: Development of oxygen carrier particles for chemical-looping combustion. Design and operation of a 10 kW chemical-looping combustor. In *Greenhouse Gas Control Technologies 7*; Rubin, E. S., Keith, D. W., Gilboy, C. F., Wilson, M., Morris, T., Gale, J., Thambimuthu, K., Eds.; Elsevier Science Ltd: Oxford, 2005; pp 115-123.
- (23) Linderholm, C.; Abad, A.; Mattisson, T.; Lyngfelt, A.: 160 h of chemical-looping combustion in a 10 kW reactor system with a NiO-based oxygen carrier. *Int. J. Greenhouse Gas Control* **2008**, *2*, 520-530.
- (24) Linderholm, C.; Mattisson, T.; Lyngfelt, A.: Long-term integrity testing of spray-dried particles in a 10-kW chemical-looping combustor using natural gas as fuel. *Fuel* **2009**, *88*, 2083-2096.
- (25) Rydén, M.; Lyngfelt, A.; Mattisson, T.: Chemical-looping combustion and chemical-looping reforming in a circulating fluidized-bed reactor using Ni-based oxygen carriers. *Energy Fuels* **2008**, *22*, 2585-2597.